Seventh Framework Programme
Theme 6 [SPACE]

# Project: 607193 UERRA

Full project title:
**U**ncertainties in **E**nsembles of **R**egional **Re-A**nalyses

## Deliverable D2.3

Ensemble variational DA diagnostics

| | |
|---|---|
| WP no: | 2 |
| WP leader: | MO |
| Lead beneficiary for deliverable : | MO |
| Name of author/contributors: | Peter Jermey, Jemma Davie, Richard Renshaw |
| Nature: | Report |
| Dissemination level: | PU |
| Deliverable month: | 30 |
| Submission date: December 22nd 2016 | Version nr: 1 |

# Ensemble Variational Data Assimilation Diagnostics

Peter Jermey, Jemma Davie, and Richard Renshaw

January 3, 2017

## 1 Introduction

The Met Office has completed development of the regional ensemble of reanalyses system that will be used to produce an ensemble of forty year regional reanalyses for the European domain and production has begun. The system is being used to produce an ensemble of realisations of atmospheric variables, available hourly for forty years. The set of realisations can also be used to derive mean and spread (uncertainty) for each variable.

The ensemble information will also be used to derive background error covariance statistics to drive a high resolution deterministic reanalysis for the same period. These error statistics will be synoptically dependent and are expected to be superior to static error covariance statistics. The deterministic and ensemble reanalyses are the principal contribution of the Met Office to the Uncertainties in Ensembles of Regional Reanalyses (UERRA) project, [Unden et al., 2014].

This document is a report on diagnostics of the ensemble system which demonstrate the validity and quality of the production. Section 2 details aspects of the system design and development. Observation monitoring, assimilation statistics and verification statistics are detailed in Sections 3, 4 and 5, respectively. The report is summarised in Section 6.

## 2 Ensemble System

Each member of the ensemble is produced by a cycled forecast using the Met Office Unified Model, [Davies et al., 2005], with the Even Newer Dynamics dynamical core (ENDGame), [Wood et al., 2014]. The forecast is initialised three hours before the analysis time and runs for a further nine hours beyond the analysis time to provide a background state for the subsequent cycle. An analysis increment to the background is calculated by 4DVAR data assimilation, [Rawlins et al., 2007], which estimates the optimal atmospheric state given the observations and background state within a six hour window. Hourly output atmospheric fields are available via reanalyses every six hours and (re)forecasting from these reanalyses to obtain hourly fields in between these times. The cycling system is shown in figure 1 and a full list of output fields is

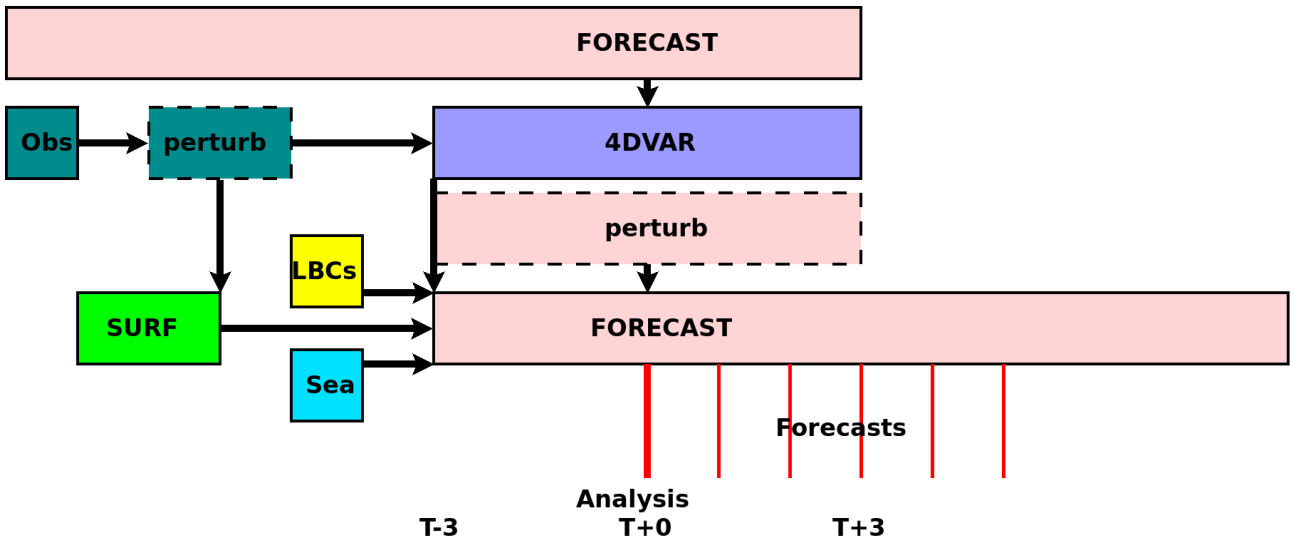


Figure 1: Diagram of ensemble member cycling.

available in appendix B.

The members of the ensemble are isolated from one another, with no re-centering of the ensemble at analysis time. Such a system has the advantage that further members can be introduced at a later date. Each member receives a different realisation of the observations, a different realisation of the model and a different realisation of the boundary conditions. In addition an unperturbed control member is run to perform operations for the ensemble: observations archive extraction and format conversion, observation blacklisting using the new Monitoring and Updating Station Lists (MUSLi) system, providing a guess state for the ensemble 4DVAR analyses and performing variational bias correction for the satellite data, [Lorenc, 2012], [Dee, 2004], (VarBC).

For each member, each observation is randomly perturbed with its own error estimate. Drawing on previous work to diagnose model error, [Piccolo and Cullen, 2016], the model is perturbed by adding a random analysis increment from a previously calculated archive. An analysis increment can be assumed to be drawn from the same distribution as model error if analyses are drawn from the same distribution as the truth.

## 2.1 Boundary Conditions

Regional models require boundary conditions over land, over sea, at the top of the model and at the lateral boundaries. For all members, the boundary at the top of the model (approximately 40km) is a solid lid i.e. the vertical gradient of all modelled variables is zero.

| Period | Member $i$ | Control |
|---|---|---|
| 01/1979 - 08/2010 | HadISST2$_i$ % 10 | HadISST2$_\mu$ |
| 09/2010 - 12/2016 | OSTIA + HadISST2$^r_i$ % 10 - HadISST2$^r_\mu$ | OSTIA |

Table 1: Sea boundary conditions for ensemble reanalysis. Subscript $i$ indicates member number and superscript $r$ indicates a random date.

### 2.1.1 Sea boundary

The two elements which vary in the sea boundary are the sea surface temperature (SST) and the fraction of sea ice. These are provided for the most part by the Hadley Centre Ice and Sea Surface Temperature data set version 2, [Titchner and Rayner, 2014], (HadISST2). Since this is an ensemble data set no additional perturbation is necessary. This data is not available beyond 2010 and so for the modern period 2010-2016 the Met Office Operational Sea Surface Temperature and Sea Ice Analysis, [Donlon et al., 2012], (OSTIA) is used, degraded to the resolution of HadISST2 and perturbed by perturbations from HadISST2 randomly drawn from an archive (matching month, but not year). This arrangement is shown in table 1.

### 2.1.2 Land boundary

The land boundary is provided by the Met Office Land Surface Data Assimilation System, [Candy, 2014], (SURF) used in a regional context for the first time. As with the atmospheric analysis, each member of the ensemble performs its own land surface analysis from a different realisation of in-situ observations. Along with VarBC, this is the first time SURF has been used in a regional context and so these two regional systems were trialled against a control ensemble using reconfigured global soil moisture and static satellite bias correction.

Figure 2 shows a comparison of the trialled system using regional SURF and regional VarBC against a control using reconfigured global soil moisture and static satellite bias correction. The figure shows ensemble diagnostics (rank histogram, estimate of mean RMSE and spread)in 1.5m temperature and 10m wind vector. These results show that the regional systems give an increase in spread for 1.5m temperature and a slight increase in spread for 10m wind vector. This is expected since each member in the control system is constrained to the same land surface boundary. The results also show a small increase in error in 1.5m temperature.

### 2.1.3 Lateral boundaries

It was originally intended that the lateral boundary conditions (LBCs) should be provided by the ensemble data set from the European Centre for Medium Range Weather Forecasting's (ECMWF) fifth Reanalysis (ERA5), [Dee, 2014]. Production on ERA5 was delayed so that use of this data was no longer viable for this project. To measure the impact of reverting to static boundary conditions provided by ECMWF's ERA-Interim, [Dee et al., 2011], another short trial

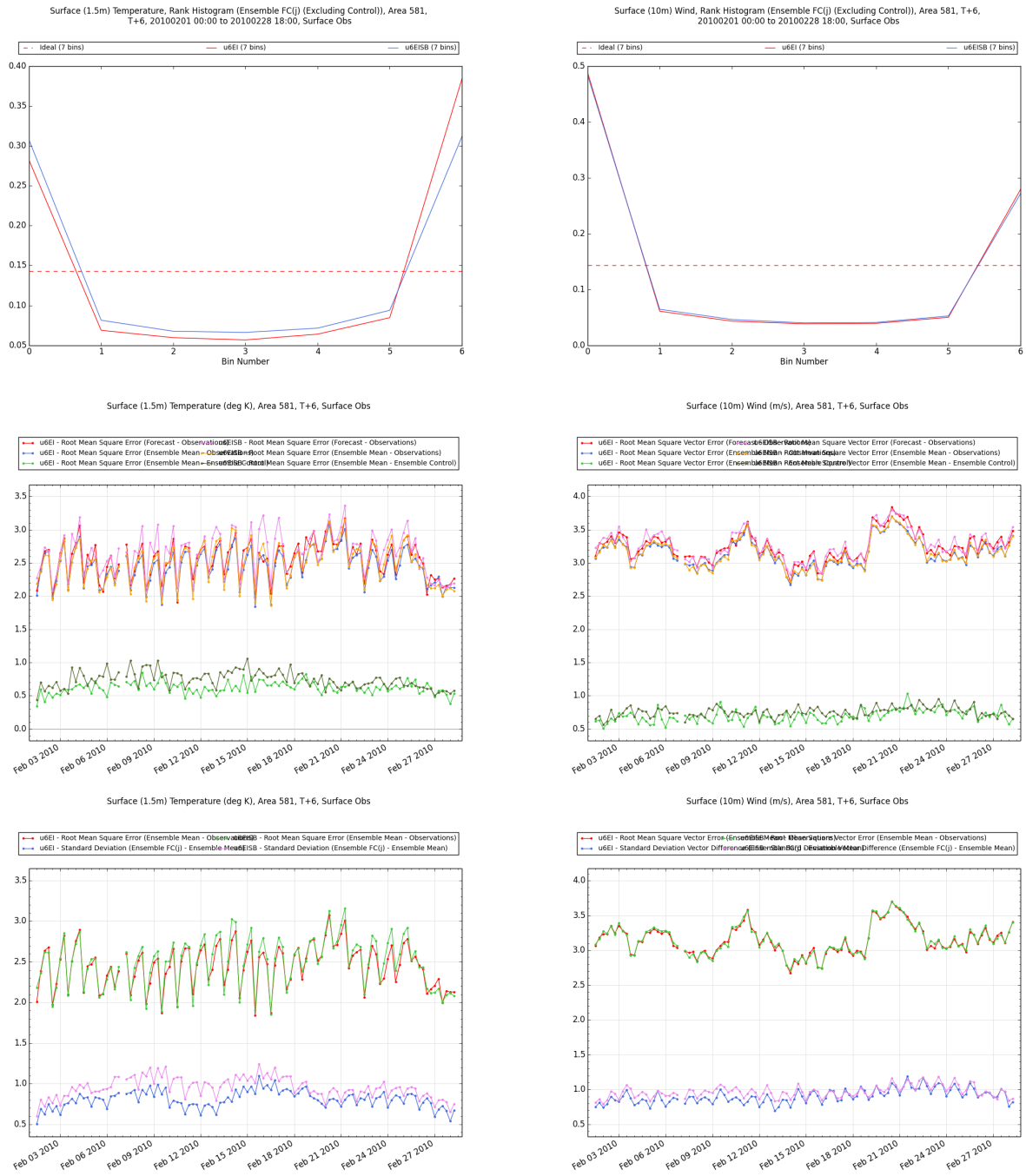


Figure 2: Comparison of ensemble using regional SURF & VarBC against that using reconfigured global soil moisture and static satellite bias correction. Left-hand plots compare (re)forecasts from the reanalyses with observations of 1.5m temperature. Right-hand plots compare (re)forecasts from the reanalyses with observations of 10m wind. The top row shows rank histograms for trial (blue) and control (red). The middle row shows RMS difference of the control wth observations, the mean with observations and the control with the mean for trial (pink, orange, dark green, respectively) and control (red, blue, light green, respectively). The bottom row shows RMS differences of the mean with the observations and the spread of the ensemble for trial (green and pink, respectively) and control (red and blue, respectively).

was performed comparing the performance of the ensemble using ensemble LBCs from ERA5 against deterministic LBCs from ERA-Interim.

Figure 3 shows a comparison of the ensemble using ensemble LBCs from ERA5 with the ensemble using deterministic LBCs from ERA-Interim. Again, the figure shows ensemble diagnostics in 1.5m temperature and 10m wind vector. These results show that the spread in the ensemble is only slightly reduced moving from ensemble LBCs to deterministic LBCs and this move also causes a slight reduction in error.

Figure 4 shows RMS difference with observations and spread for several flavours of ensemble: perturbed LBCs (ERA5) only, perturbed model & LBCs only and perturbed model & LBCs & observations. The results show that perturbed LBCs cause some spread within the ensemble, but that the majority of the spread in the ensemble is due to the model perturbations. RMS difference with analysis seems comparable between the three systems.

### 2.2 Ensemble size

It was originally intended to have an ensemble size of 20 members. Experiments to investigate the ensemble spread dependency on ensemble size were carried out to demonstrate the need for this size of ensemble. Some results are shown in figure 5. This figure shows that increasing ensemble size increases spread and that the larger the ensemble size the smaller the impact of adding new members. This is expected since it is well known that at short forecast times spread is dependent on ensemble size, [Buizza and Palmer, 1998]. Therefore the production has begun with 20 members.

### 2.3 Summary

A summary of the production system is given in table 2.

## 3 Observation Monitoring Statistics

Station statistics comparing background (six hour forecast) with the observed values (O-B) are used by MUSLi to make automatic decisions whether to assimilate observations from the station, or to reject or correct the observations before assimilation during the following month. These decisions are used for updating station assimilation blacklists within the MUSLi system. An example of these statistics is shown in figure 6, which shows the spatial variation in bias and standard deviation of 2m temperature O-B values at all SYNOP stations for May 1979. These

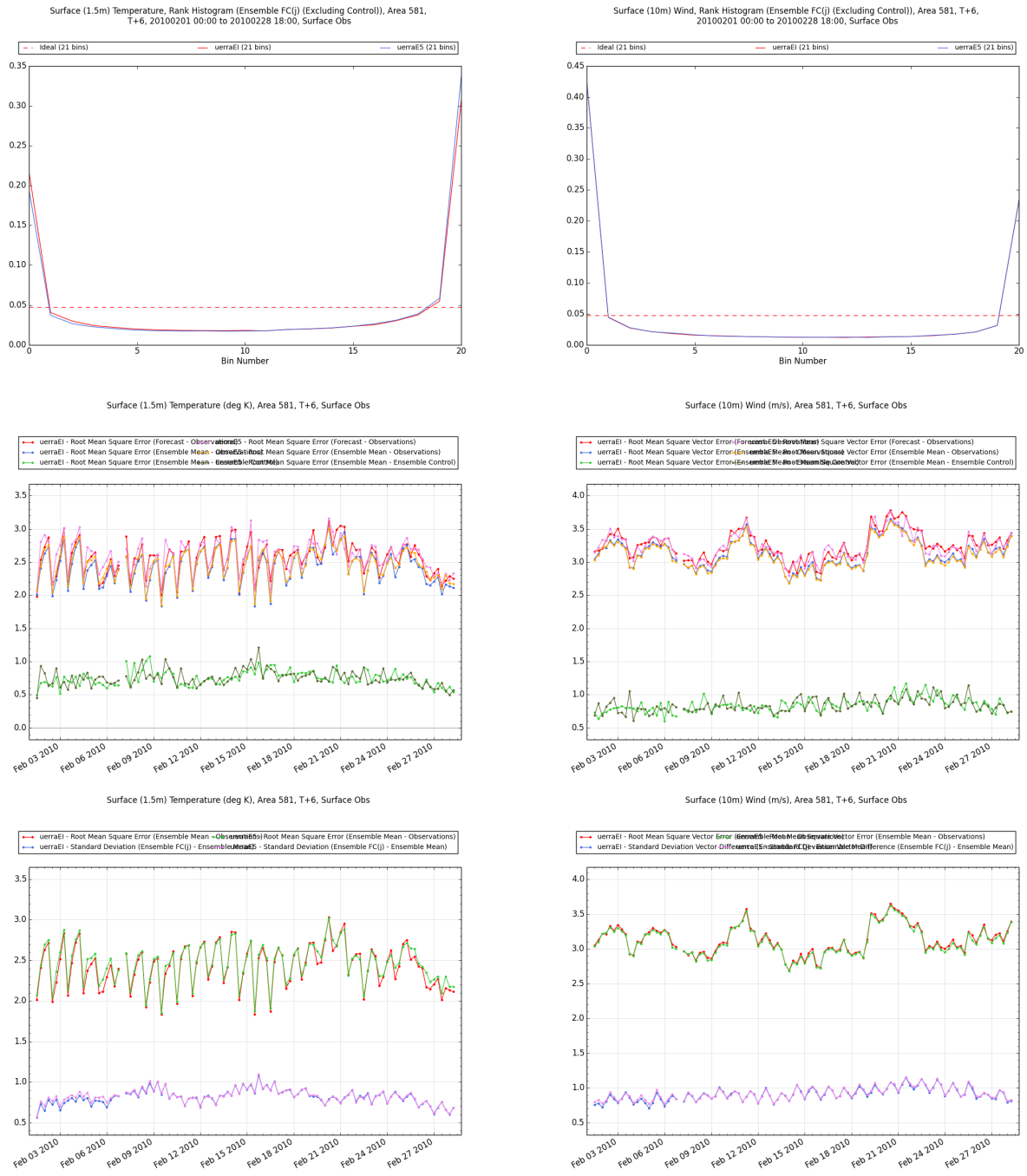


Figure 3: Comparison of ensemble using LBCs from ERA5 with that using LBCs from ERA-Interim. Left-hand plots compare (re)forecasts from the reanalyses with 1.5m temperature observations. Right-hand plots compare (re)forecasts from the reanalyses with 10m wind observations. The top row shows rank histograms for ERA5 LBCs (blue) and ERA-Interim LBCs (red). The middle row shows RMS difference of the control with observations, the mean with observations and the control with the mean for ERA5 LBCs (pink, orange, dark green, respectively) and ERA-Interim LBCs (red, blue, light green, respectively). The bottom row shows RMS differences of the mean with observations and ensemble spread for ERA5 LBCs (green and pink, respectively) and ERA-Interim LBCs (red and blue, respectively).

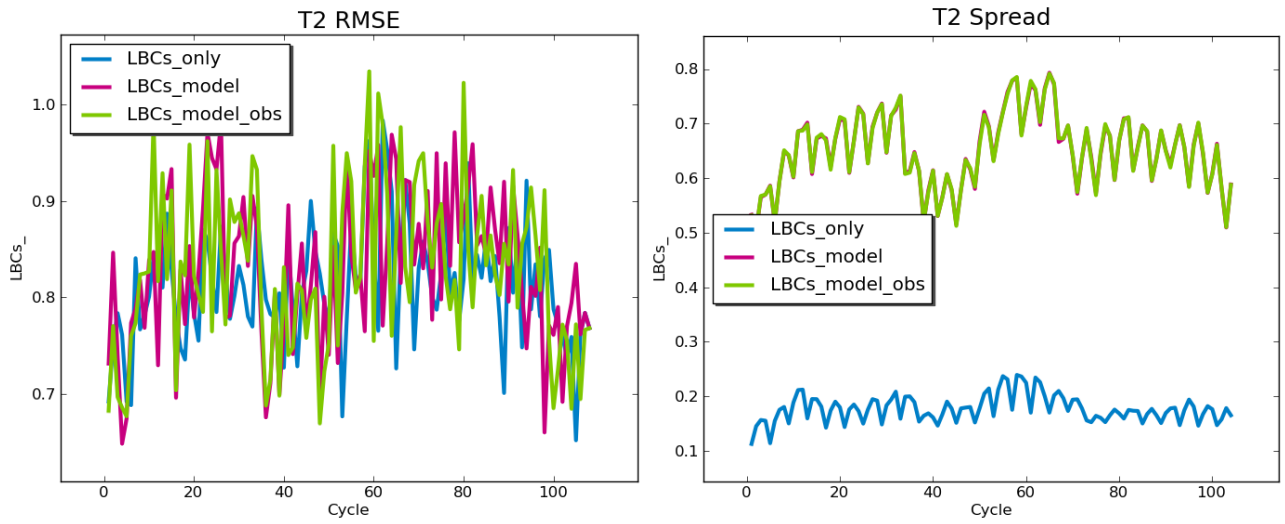


Figure 4: Comparison of 1.5m temperature forecast (T+6) from (6 member) ensemble with perturbed LBCs only (blue), perturbed model & LBCs (pink) and perturbed observations & model & LBCs (green). The left hand plot shows RMS difference of the mean with a random member analysis and the right hand plot shows spread.

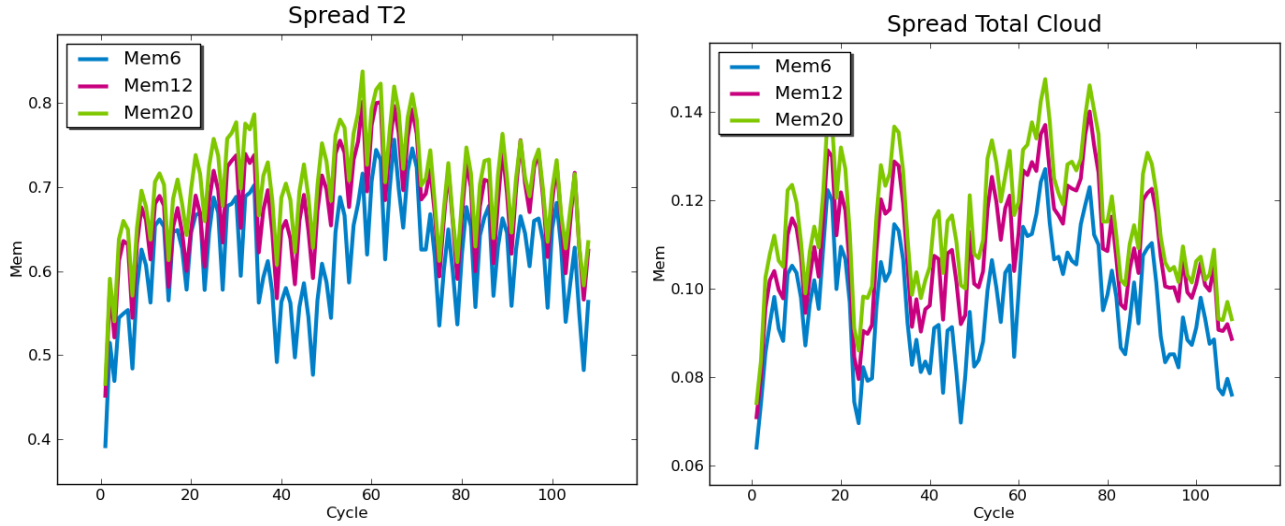


Figure 5: Comparison of spread in forecast (T+6) from ensemble with 6 (blue), 12 (pink) and 20 (green) members. The left hand plot shows spread in 1.5m temperature and the right in total cloud.

| Item | System |
|---|---|
| Model | UM |
| Dynamical Core | ENDGame |
| Resolution | $0.33 \circ \approx 33km$ |
| Atmospheric Assimilation | 4DVAR |
| Assimilation Resolution | $0.66 \circ \approx 66km$ |
| Land Assimilation | SURF (EKF) |
| Sea Boundary | HadISST2 |
| Lateral Boundary | ERA-Interim (not perturbed) |
| Observations | ERA-Interim, plus ground GPS, plus scatterometer winds, randomly perturbed |
| Model perturbations | Random analysis increments |
| Ensemble size | 20 |

Table 2: Summary of ensemble production system.

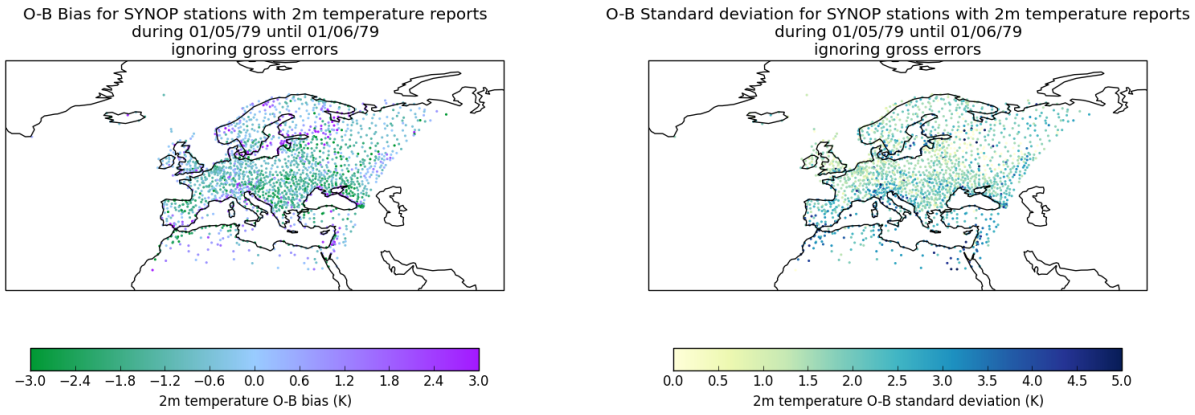


Figure 6: Maps of SYNOP station 2m temperature O-B bias values (left) and standard deviation values (right) for ensemble control for May 1979. Statistics have been calculated ignoring reports with O-B values outside gross error thresholds.

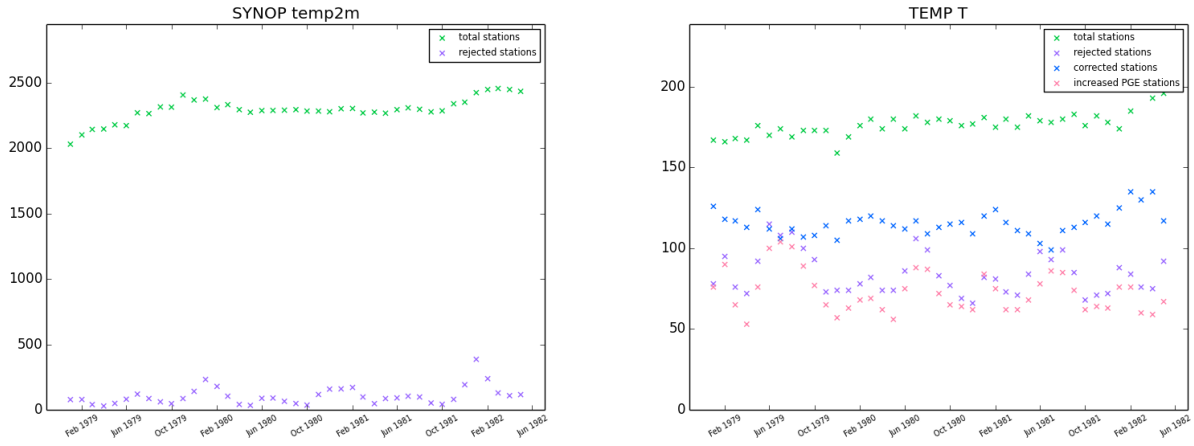


Figure 7: Time series of number of reporting stations (green), rejected stations (purple), stations with increased probability of gross error (pink) and corrected stations (blue) 1979-1982. Left - surface stations, right TEMP sondes.

plots suggest that there is no spatial bias comparing the model against the observations. The bias and standard deviation calculations ignore observations with gross errors as these observations would be rejected by quality control and are not necessarily an indicator of the overall quality of observations from the station.

Figure 7 shows time-series of observation monitoring statistics for the control system. This shows that there are a large number of available surface stations of acceptable quality, with relatively few stations being rejected. There are also a large number of sondes in the domain, but many of these require bias correction or are partially or fully rejected. The figure suggests there is some seasonal dependency, with more surface stations being rejected in winter and more sondes rejected in summer.

# 4 Assimilation Statistics

Figure 8 shows the observation penalty of the background (six hour forecast). This penalty is a combination of the RMS differences of the six hour forecast from the reanalysis with observations of each assimilated type and is therefore a proxy for the error of the reanalysis multiplied by the number of observations. This figure demonstrates that the quality of the ensemble of reanalyses is consistent for most of the period, both across the three months shown here and across individual members (since the spread of observation penalties is low). There are a number of cycles of the reanalysis in which the observation penalty is very low and this corresponds to low observation availability at these date/times. There is a larger value of the observation penalty of the background after the longest period of these observation dropouts. This suggests that,

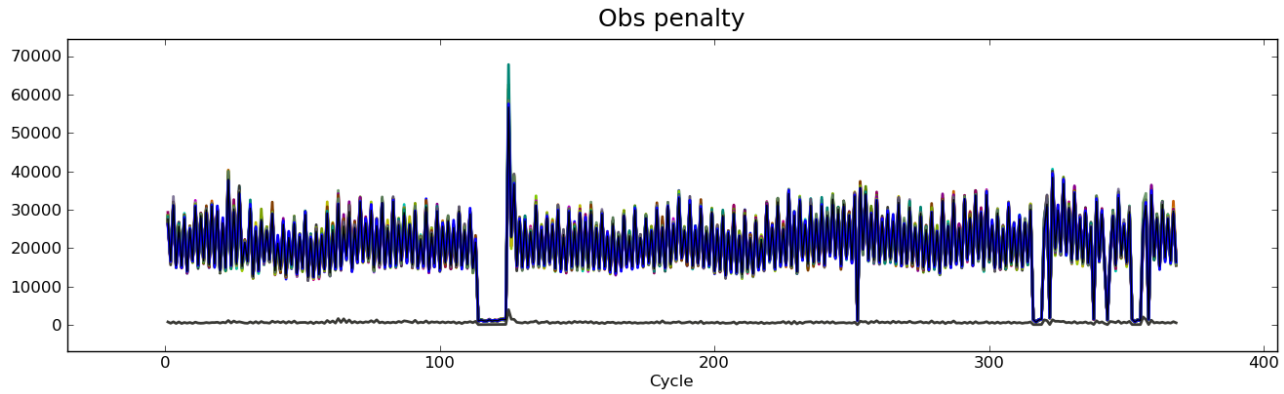


Figure 8: Observation penalty of the background which is a combination of RMS differences between the background and observations of all assimilated types. Each member's statistics is shown by a coloured line, the mean and the spread of values are thin and thick black lines, respectively. Statistics are shown for March, April and May 1979.

without many observations to constrain it, the reanalysis has drifted further from the true state.

Figure 9 shows the total penalty of the analysis and the number of iterations of the 4DVAR minimisation required for convergence. The penalty is a measure of the distance of the analysis from the background state and the assimilated observations. The total penalty is relatively stable, occasionally reaching low values due to a sudden reduction in assimilated observations and some larger values after observations are restored. The spread of values is consistently very low, but shows some difference between different members. Likewise the number of iterations required for convergence is relatively stable except for occasional low values, some of which correspond to low total penalties.

Figure 10 shows the observation and background penalties of the analysis, which are the principal components of the total penalty. The observation and background penalties are measures of the distance of the analysis from the observations and backgrounds, respectively. Both penalties shown reflect the total penalty and are, therefore, relatively consistent except for a few cycles for which the penalties are very low, again reflecting the small number of available observations.

Figure 11 shows the highest value of the high frequency penalties for each cycle. These are secondary penalty components designed to penalise spuriously high atmospheric frequencies. Unusually high values of these penalties at any point in the minimisation algorithm may indicate problematic or false convergence, which may lead to a poor quality reanalysis. The figure shows that behaviour of both statistics is relatively consistent throughout the period for all ensemble members. There are occasionally high penalties for individual ensemble members, but these are not so large as to indicate difficulties with convergence.

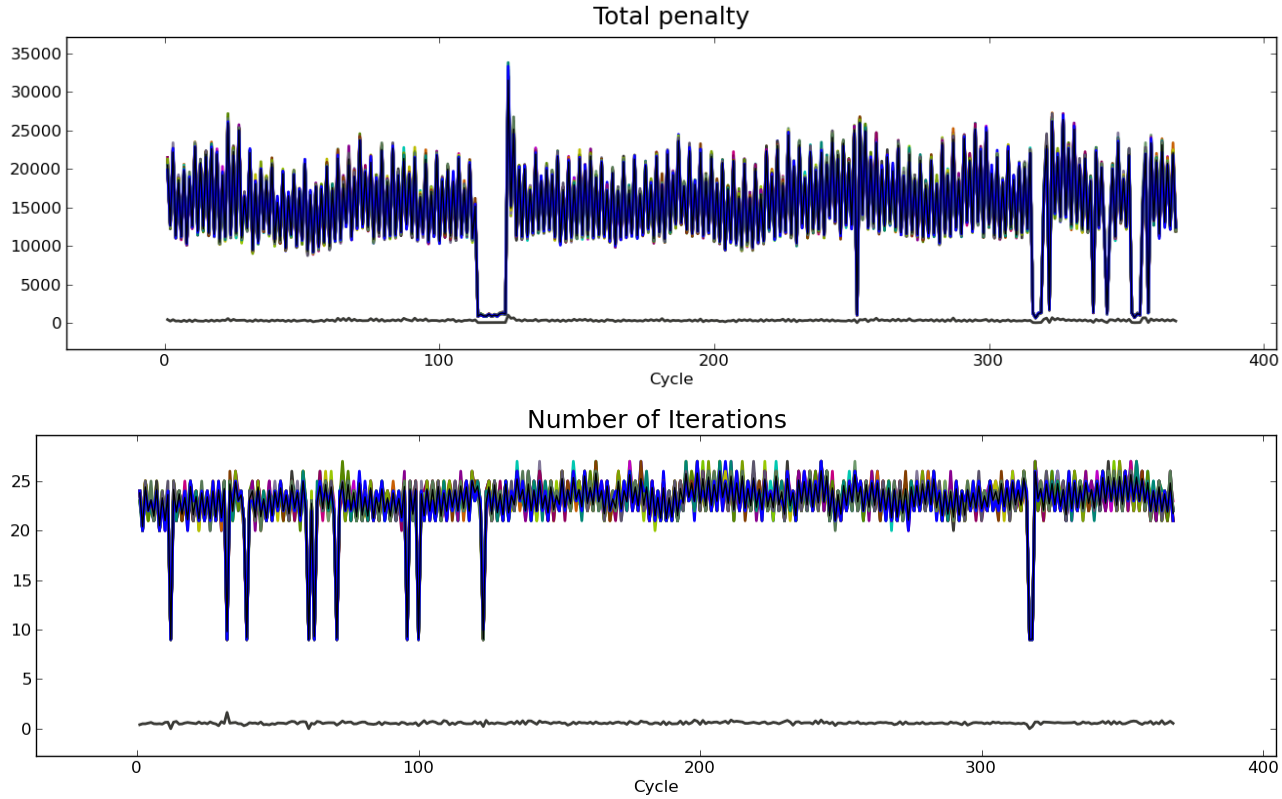


Figure 9: Assimilation Statistics: The top plot is the total penalty of analysis and the bottom plot is number of iterations required for convergence. Each member's statistics is shown by a coloured line, the mean and the spread of values are thin and thick black lines, respectively. Statistics are shown for March, April and May 1979.

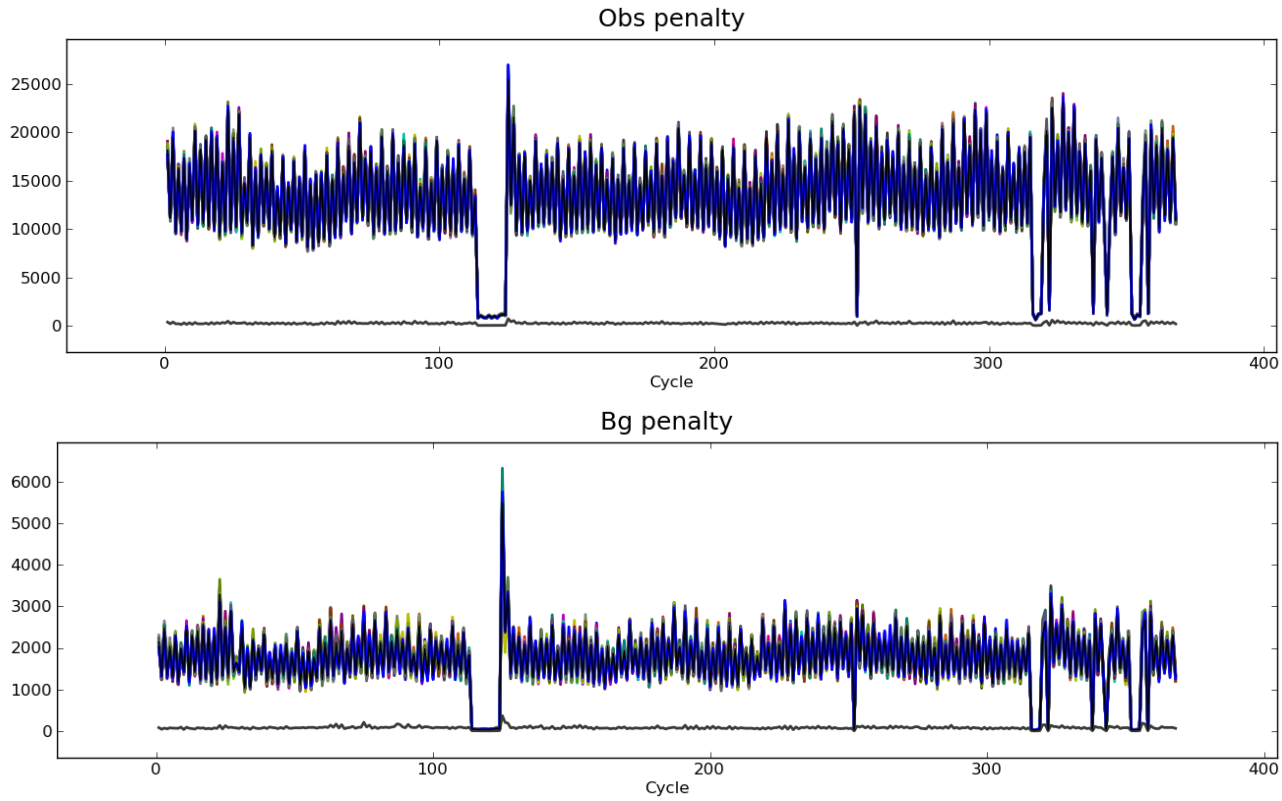


Figure 10: Assimilation Statistics: The top plot is the observation penalty of the analysis and the bottom plot is the background penalty of the analysis. Each member's statistics is shown by a coloured line, the mean and the spread of values are thin and thick black lines, respectively. Statistics are shown for March, April and May 1979.

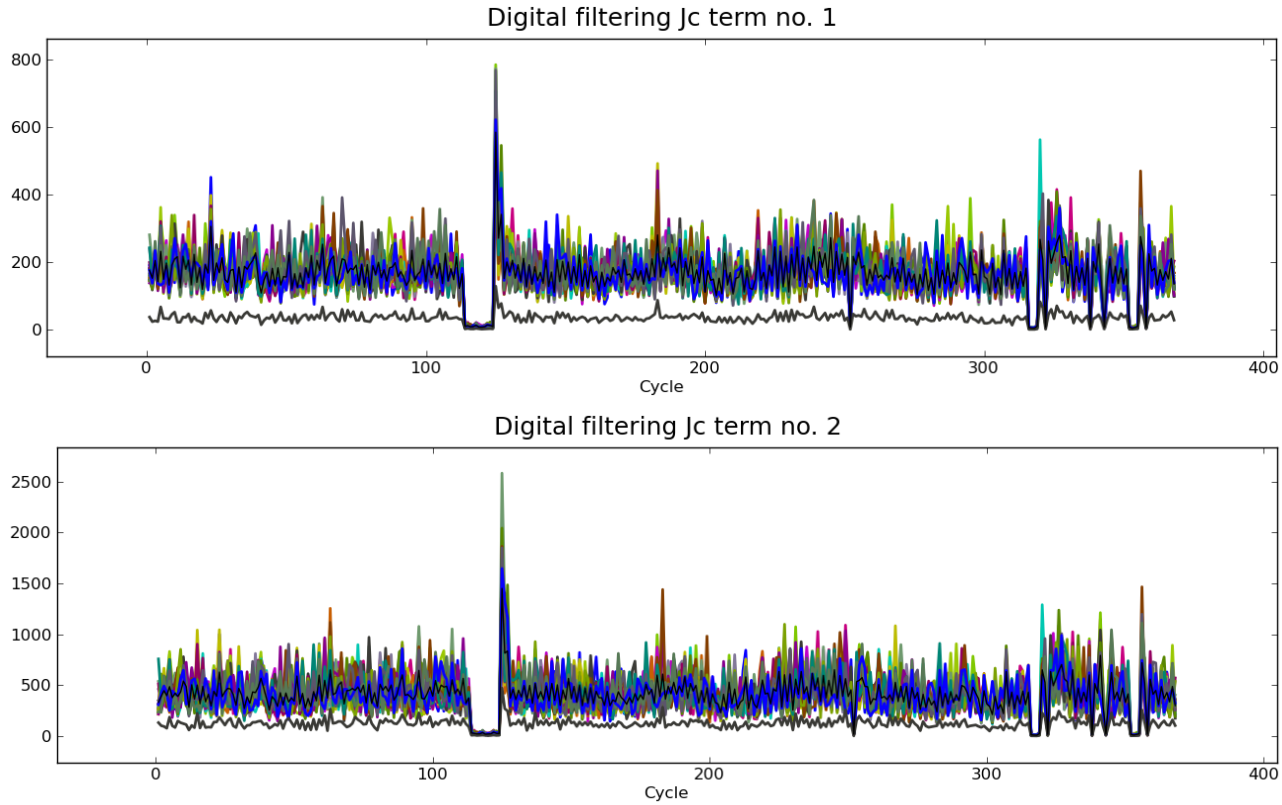


Figure 11: Assimilation Statistics: Top and bottom plots show the largest first and largest second high frequency penalties, respectively, on each cycle. Each member's statistics is shown by a coloured line, the mean and the spread of values are thin and thick black lines, respectively. Statistics are shown for March, April and May1979.

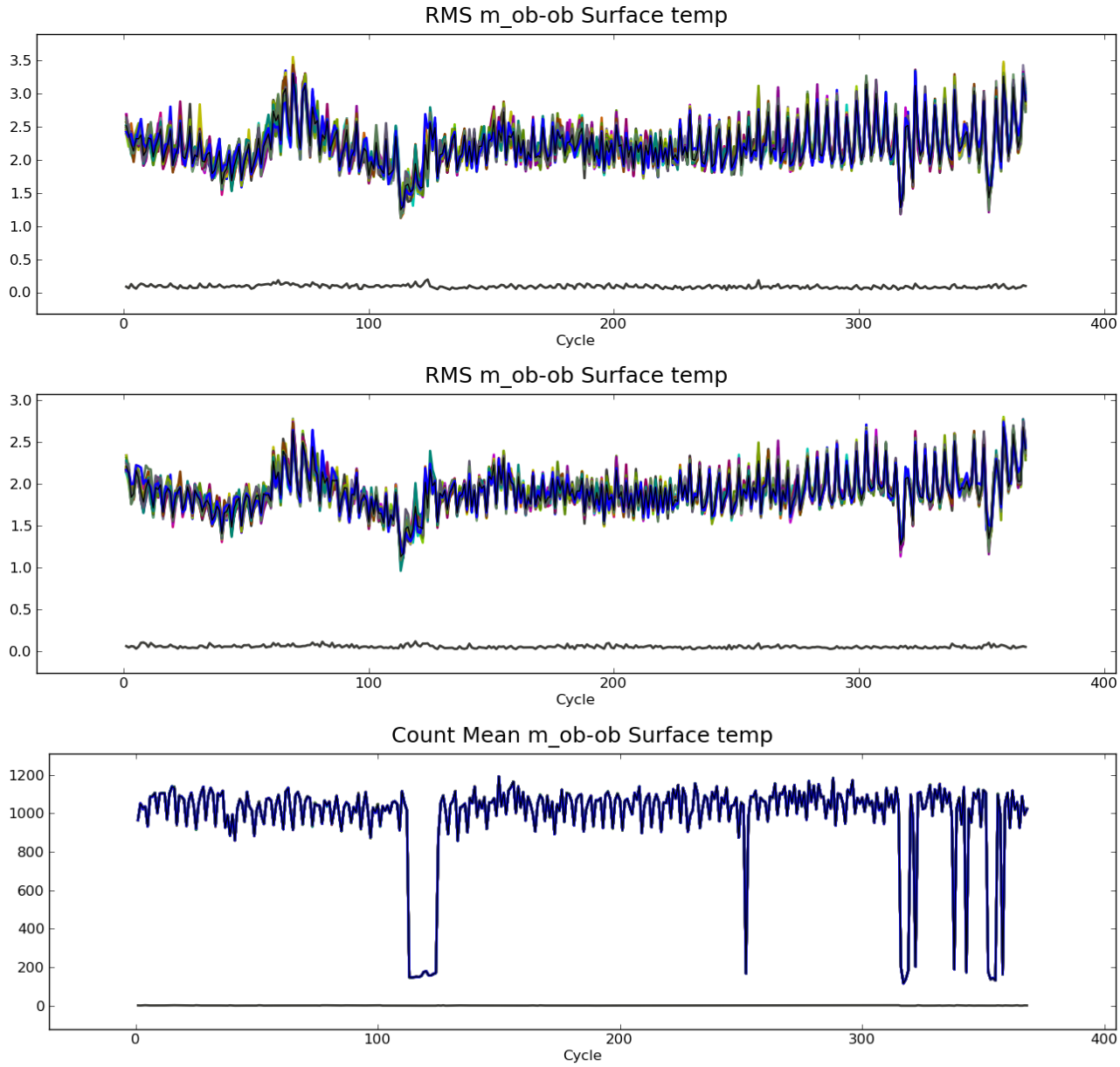


Figure 12: Assimilation Statistics for SYNOP station temperature observations: The top plot shows the RMS difference between observations and the background, the middle plot shows the RMS difference between the observations and analysis and the bottom plot shows the count of assimilated observations. Each member's statistics is shown by a coloured line, the mean and the spread of values are thin and thick black lines, respectively. Statistics are shown for March, April and May.

The bottom plot of figure 12 shows the count of station temperature observations assimilated by each member of the reanalysis. This figure demonstrates the variance of the number of observations available in the archive. For most of the period shown around a thousand stations are assimilated, but there are several cycles on which the number of available observations is as low as of the order of a hundred. The number of assimilated observations varies little between ensemble members.

The top plot of figure 12 shows the RMS difference between the background and the observations. This is a measure of error in the six hour forecast from the ensemble of reanalyses, taking station temperature observations as truth. The RMS difference with the background suggests that all members are reasonably consistent with the observations throughout the period. The RMS difference decreases on the occasions where the available observations are few, which is misleading. Doubtless the quality of the reanalysis diminishes for these cycles, but consistency with the available observations remains good. Similar results are shown by the middle plot of figure 12 which is the RMS difference between the analysis and the observations, which is a measure of the fit of the analysis to the observations. These differences are slightly lower than those of the background indicating that the assimilation has drawn the state closer to the observations.

The same statistics are shown for sonde wind observations in figure 13. The number of available sondes varies between 19 and 122. This is a large range, but not as large as that of the station observations. The consistency of the RMS differences between the observations and the background and the analyses is good. Again the differences between the observations and the analyses are smaller than between the observations and the background because the assimilation has drawn the state towards the observations.

Assimilation statistics are shown for aircraft wind observations in figure 14. The RMS difference between observations and the background and observations and the analysis again remains relatively consistent for the period show except for a few cycles where these values become small and a two cycles where they become large. The cycles where the differences are unusually small correspond to cycles with few available observations. The cycles where the differences are unusually large correspond to cycles with very few station observations, indicating a decrease in quality for these cycles.

# 5 Results

## 5.1 Month Average Spread

Figure 15 shows the mean values of the ensemble mean and spread over March 1979 for 1.5m temperature, 10m wind speed and six-hourly precipitation. The reanalysis spread is greatest over complex orography for 1.5m temperature, over the sea for 10m wind speed and where there is high precipitation and complex orography for precipitation. This is as expected for the re-

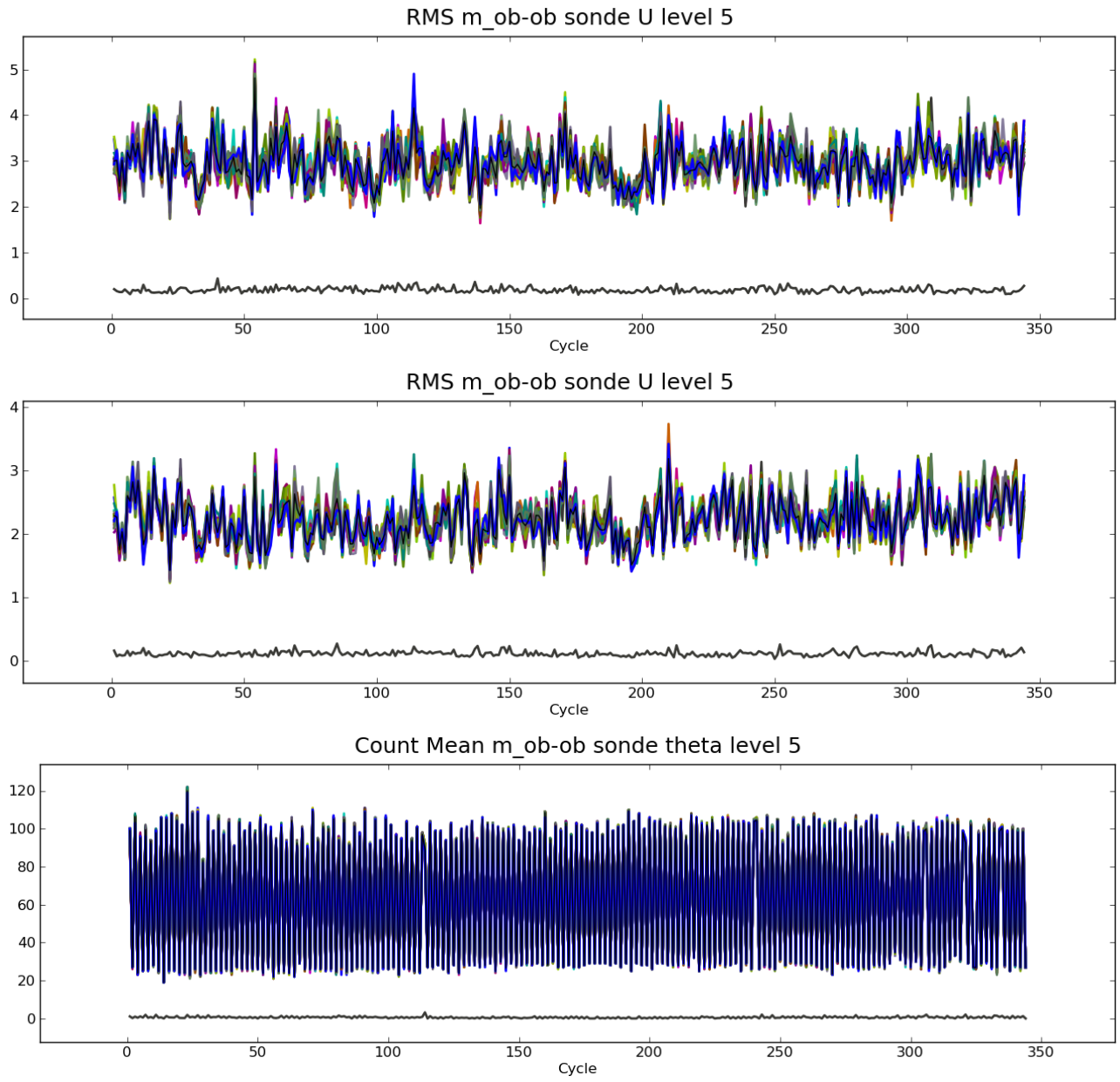


Figure 13: Assimilation Statistics for level 5 sonde wind observations: The top plot shows the RMS difference between observations and the background, the middle plot shows the RMS difference between the observations and analysis and the bottom plot shows the count of assimilated observations. Each member's statistics is shown by a coloured line, the mean and the spread of values are thin and thick black lines, respectively.

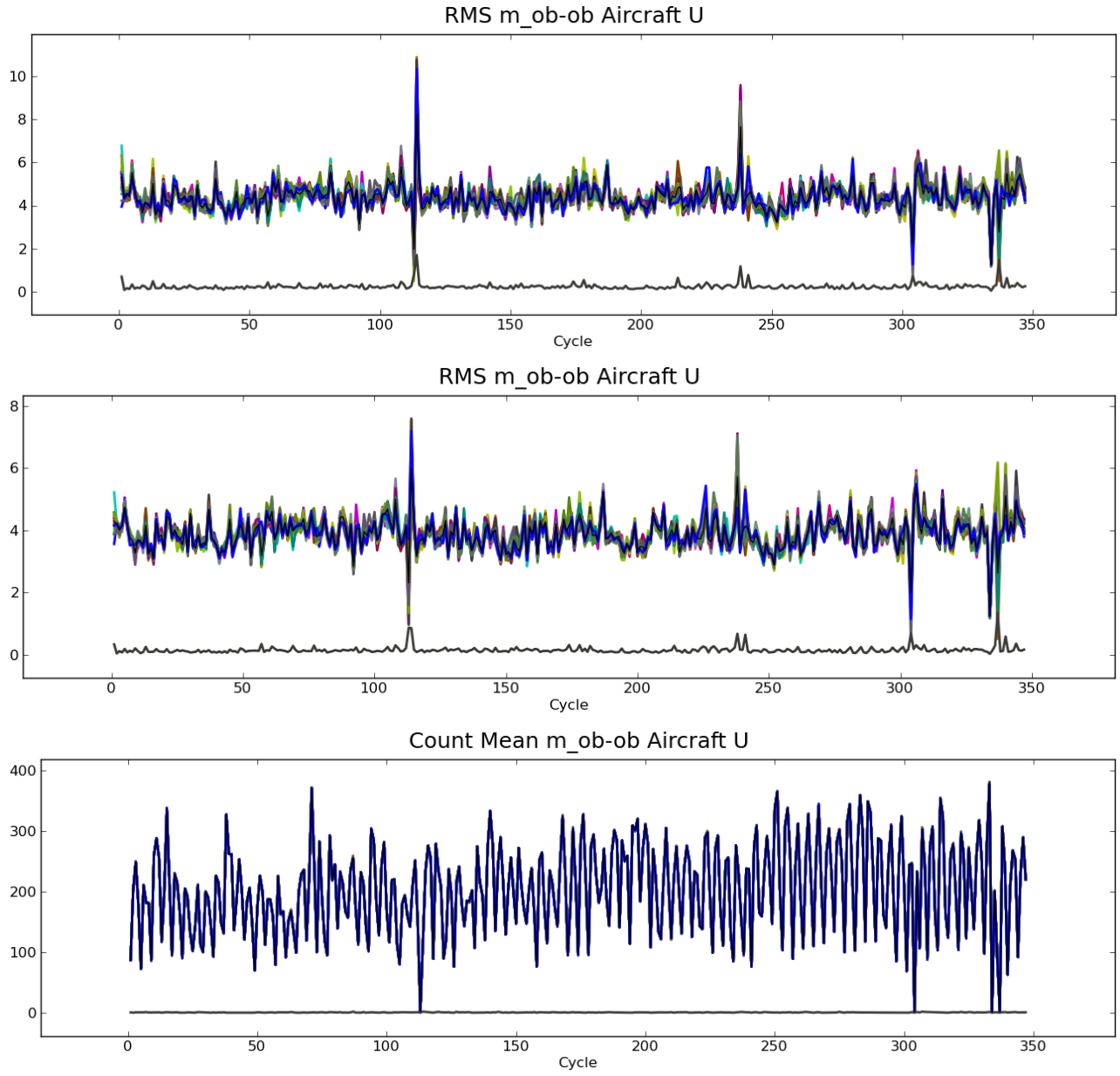


Figure 14: Assimilation Statistics for aircraft wind observations: The top plot shows the RMS difference between observations and the background, the middle plot shows the RMS difference between the observations and analysis and the bottom plot shows the count of assimilated observations. Each member's statistics is shown by a coloured line, the mean and the spread of values are thin and thick black lines, respectively.

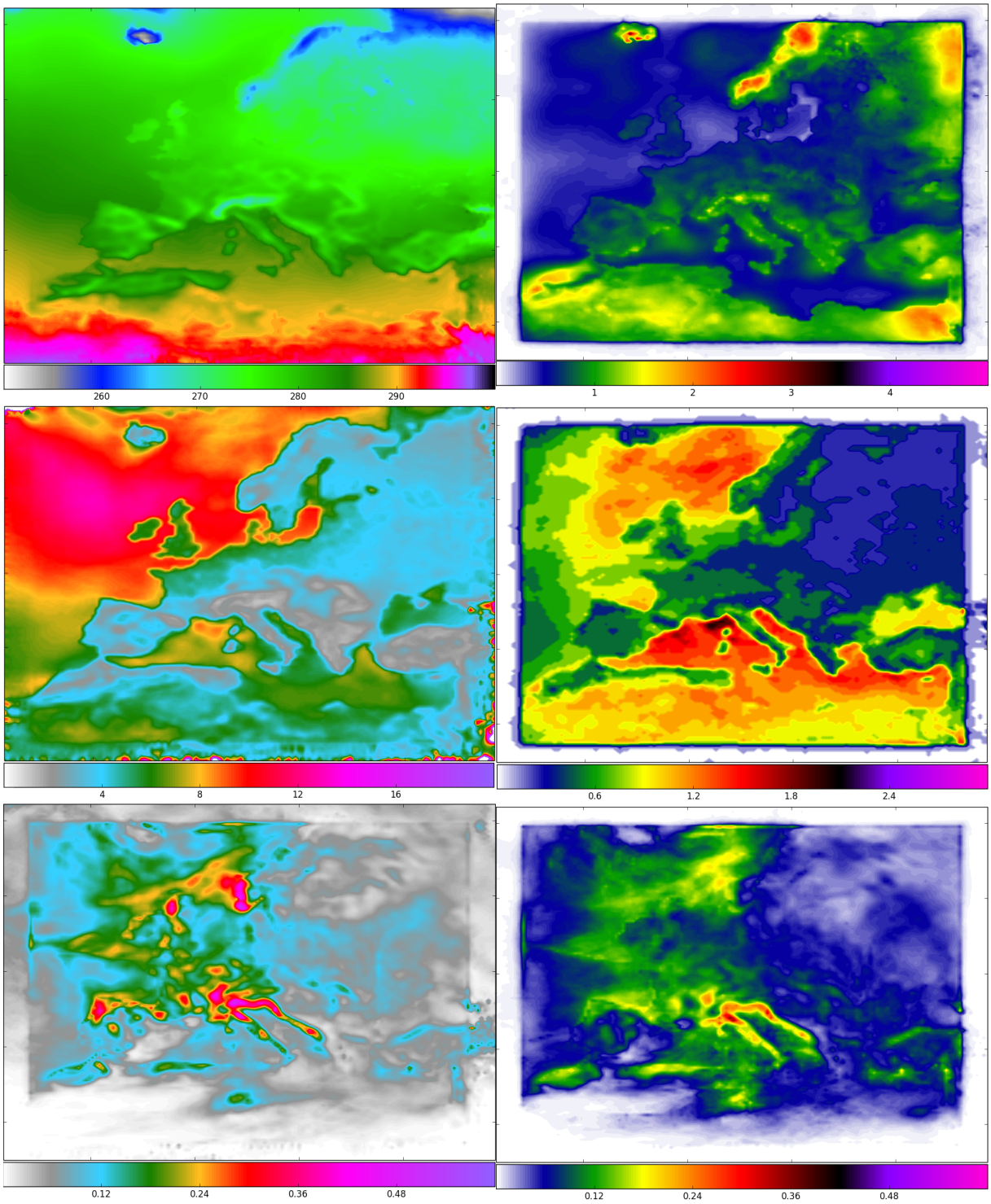


Figure 15: Mean of ensemble mean values over March 1979 (left hand side), together with mean spread over the same period (right hand side). The top row shows 1.5m temperature, the middle shows 10m wind speed and the bottom row shows six-hourly precipitation.

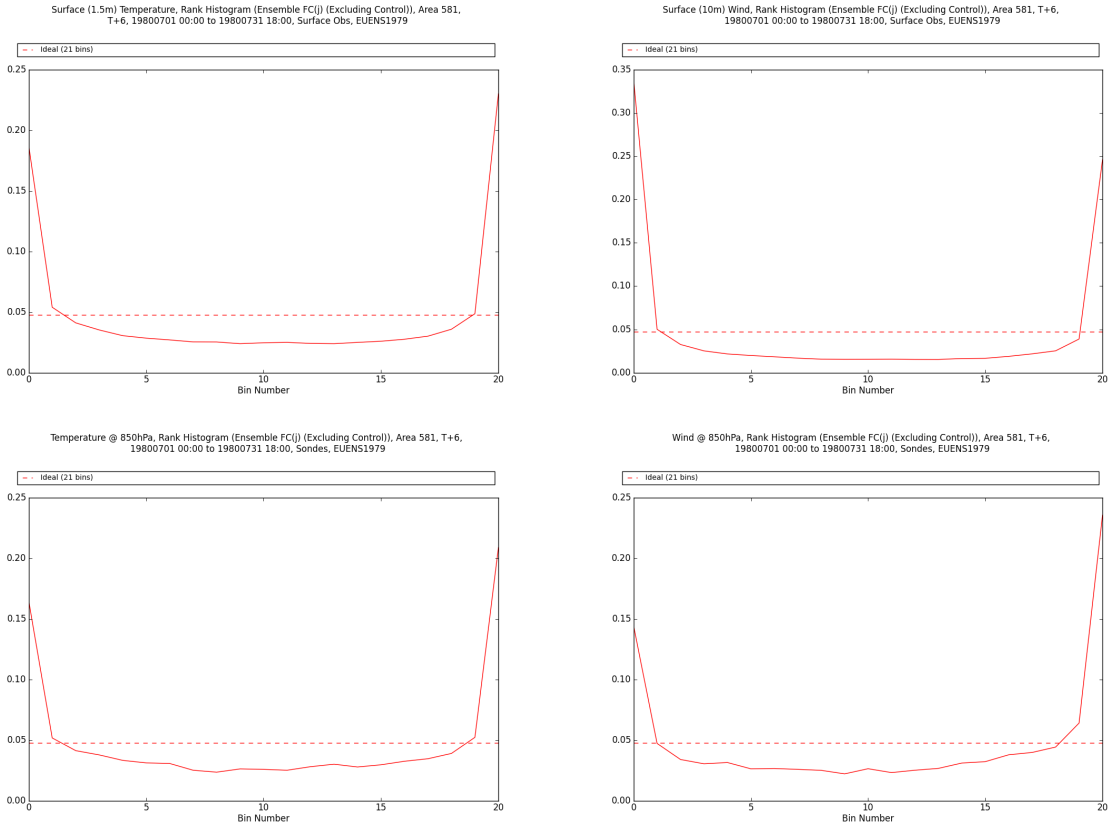


Figure 16: Rank histograms of observations against reanalysis ensemble members. The top row shows 1.5m temperature and 10m wind, using station observations and the bottom row shows temperature and wind at 850hPa, using sondes. July 1980.

analysis since the areas of complex orography cause uncertainty in the model for smaller scale variables and the limited availability of sea wind observations, together with larger values at sea also cause larger uncertainty.

## 5.2 Rank Histograms

Figure 16 shows rank histograms of observations against the ensemble members for the month of July 1980. The rank histograms all show the members as underspread against the observations, because observations have their own uncertainty/representativeness error, which leads to the most numerous ranks being external to the ensemble (0 and 20). Algorithms are available to account for this, [Saetra et al., 2004], and they will be explored as part of the validation activity. The ranks of the observations that are internal to the ensemble are similar, i.e. the interiors of the histograms are reasonably flat, indicating that each ensemble member is equally likely and suggesting that, when representivity is take into account, the ensemble spread is a reasonable

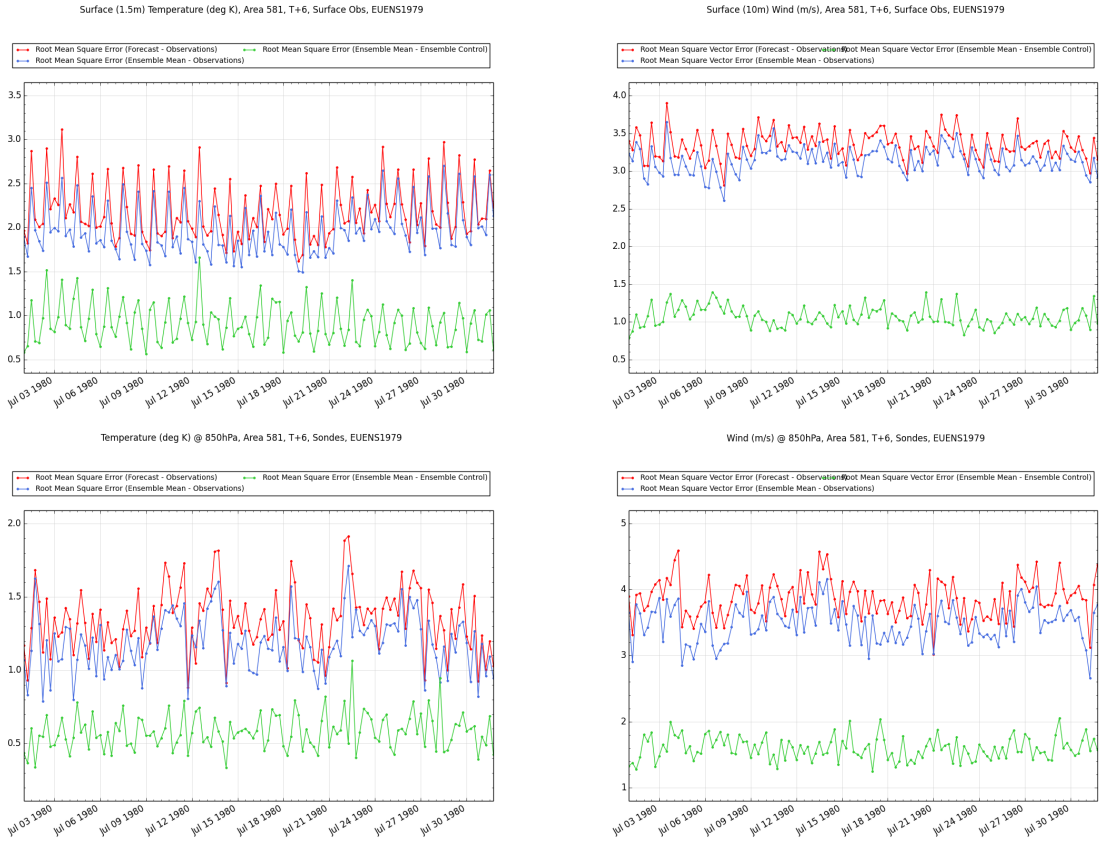


Figure 17: RMS difference of random member with observations (red), mean with observations (blue) and mean with random member (green). The top row shows 1.5m temperature and 10m wind, using station observations and the bottom row shows temperature and wind at 850hPa, using sondes. July 1980.

measure of uncertainty.

## 5.3 RMSE of ensemble mean

Figure 17 estimates the RMSE of the control, represented here by a randomly selected member of the ensemble, and ensemble mean for the month of July 1980. The plots all show that the ensemble mean has a smaller difference from observations than the control, indicating that the truth is within the spread of the ensemble. The plots suggest that the RMSE of the mean is reasonably consistent and of a reasonably small value for all variables shown.

## 5.4 Spread of the ensemble

Figure 18 compares the spread of the ensemble with the estimate of the RMSE of the ensemble mean. Again, representivity of the observations is not taken into account and so the spread

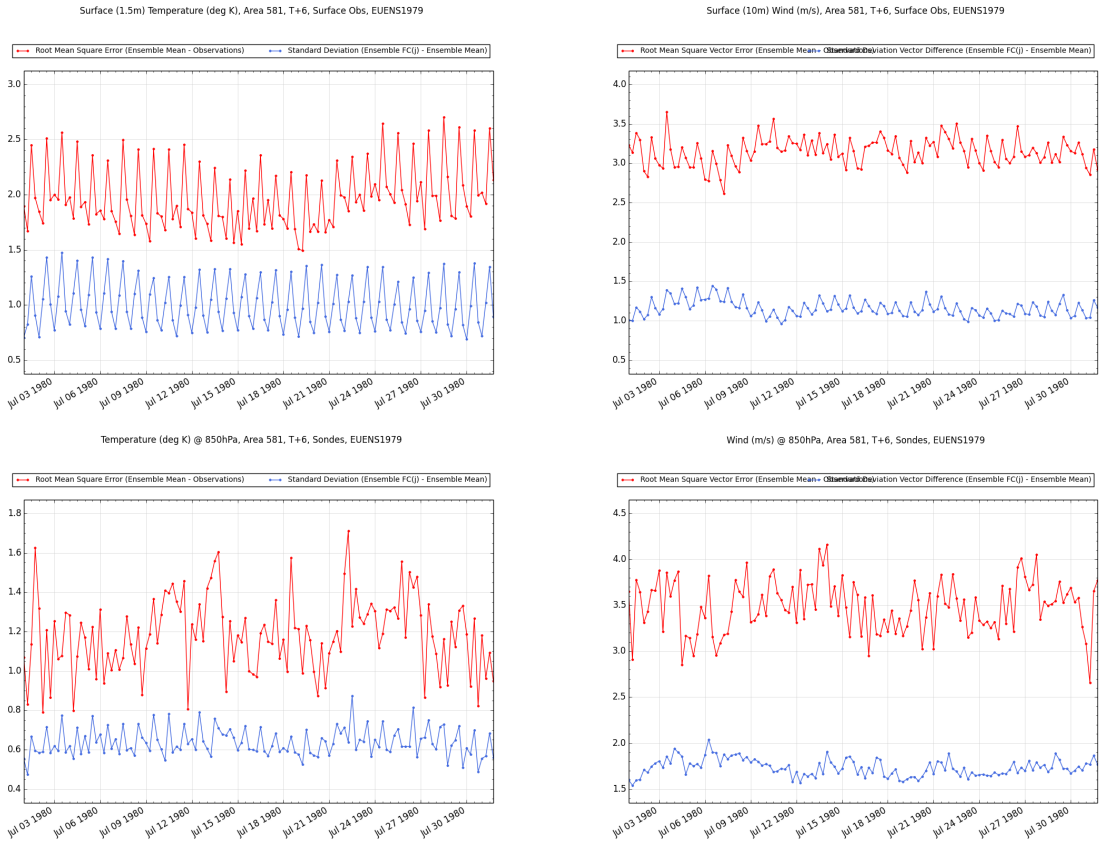


Figure 18: Spread of ensemble (blue) with RMS difference of mean and observations (red). The top row shows 1.5m temperature and 10m wind, using station observations and the bottom row shows temperature and wind at 850hPa, using sondes. July 1980.

of the ensemble appears much lower than the estimated RMSE. The ensemble spread seems to capture some, but not all, of the temporal variance in the RMSE. Most notably, peaks and troughs in the spread coincide with peaks and troughs in the RMSE across all variables shown.

# 6 Summary

The ensemble reanalysis system has been finalised and production has begun. This system is using variational bias correction and the Met Office surface analysis scheme in a regional context for the first time. Due to a delay in production of ERA5, LBCs of the ensemble are deterministic (ERA-Interim), but this has not caused a large reduction in the spread of the ensemble. The majority of the spread in the ensemble is caused by the perturbations to the model, which are provided by a random draw from an analysis increment archive.

Assimilation statistics indicate that the number of available observations is extremely low for some cycles and that this has a detrimental effect on the quality of the reanalysis.

The ensemble is producing larger uncertainty in regions where the model is known to produce less certain output (over complex orography for 1.5m temperature and precipitation and over sea for 10m wind speed). Ensemble diagnostics suggest that, as desired, each member of the ensemble is equally likely and the spread of the members encompasses the true state. The spread of the ensemble peaks when the estimate of RMSE of the mean peaks, which suggests the ensemble can be considered to be representative of the uncertainty in the mean.

Examination of the diagnostics presented here demonstrates that the ensemble is mostly behaving as expected and with reasonable consistency with the observations. The behaviour and quality of the ensemble will be examined in more detail in the validation exercise. This exercise will also employ more sophisticated diagnostics which will aim to isolate model and observation error, allowing a clearer examination of how closely the ensemble spread estimates the uncertainty.

# A Observations

The set of observations for assimilation comprises those processed for assimilation in the ECMWF reanalyses, [Dee et al., 2011], supplemented with Met Office ground global positioning (GPS) observations and scatterometer winds, as detailed in Tables 3 and 4.

Operationally at the Met Office, observation data is quality controlled before being assimilated. For the EURO4M reanalysis, a fixed 'blacklist' of observations was used for the two year period. A fixed blacklist is less appropriate for a forty year period and so the new MUSLi system is used to create new blacklists each month for surface, sonde and aircraft observations.

# B Output Fields

Model level fields are output at six-hourly reanalysis times (00Z, 06Z, 12Z and 18Z) and all other fields are output at six-hourly reanalysis times (00Z, 06Z, 12Z and 18Z) and at hourly forecast times between these.

## B.1 Multi - level fields

Model level fields are available on the UM's model levels which are a Charney-Phillips staggering between 10m above orography and the model top, which is a fixed radius from the centre of the Earth (approximately 40km above the surface). Pressure level fields are available at 1000, 975, 950, 925, 900, 875, 850, 825, 800, 750, 700, 600, 500, 400, 300, 250, 200, 150, 100, 70, 50, 30, 20 and 10hPa. Height level fields are available at 15, 30, 50, 75, 100, 150, 200, 250, 300, 400, 500m above orography. Availability of multi-level fields is given in table 5

## B.2 Radiation fields

Albedo, evaporation, surface net solar (SW) radiation, clear-sky downward solar radiation, clear-sky upward solar radiation, clear-sky downward thermal (LW) radiation, direct solar radiation, surface solar radiation downwards, surface net thermal radiation, surface thermal radiation downwards, surface sensible heat flux, surface latent heat flux and skin temperature.

## B.3 Fields at 2m above orography

Temperature, maximum temperature, minimum temperature and relative humidity

## B.4 Fields at 10m above orography

Wind speed, gust and direction.

| Observation | Subtypes | Variables | Dates | Source |
|---|---|---|---|---|
| Land SYNOP | Land synoptic observations (LNDSYN), Meteorological airfield reports (METARS), Mobile synoptic observations (MOBSYN), | Surface pressure, temperature, humidity, | 1978-2017 | ECMWF |
| SHIP | Ship synoptic observations (SHPSYN) | Surface pressure, wind, temperature, humidity | 1978-2017 | ECMWF |
| Buoy | Buoy | Surface pressure, wind, temperature | 1979-2017 | ECMWF |
| Sondes | Radiosondes (TEMP), Wind profilers (WINPRO), Dropsondes (DROPSOND), Wind only sondes (PILOT) | Upper-air wind, temperature, humidity | 1978-2017 | ECMWF |
| Aircraft | Aircraft Meteorological Data Relay (AMDARs), Air Report (AIREPs), | Flight-level temperature, | 1978-2017 | ECMWF |
| AIRS | Advanced Infared Sounder (AIRS) | AIRS | 2003-2017 | ECMWF |
| ATOVS | Global Operational Vertical Sounder (ATOVSG) | HIRS/AMSU radiances | 1998-2017 | ECMWF |

Table 3: List of observations (Part 1 of 2).

| Observation | Subtypes | Variables | Dates | Source |
|---|---|---|---|---|
| GPSRO | GPSRO | Bending Angle | 2006-2017 | ECMWF |
| Ground GPS | Integrated Water vapour (GPSIWV) | Zenith Delay | 1999-2017 | MO |
| IASI | Global (IASIG)<br>Local (IASIL) | radiances | 2007-2017 | ECMWF |
| satwinds/AMVs | ESA Cloud Motion Winds (ESACMW),<br>ESA High Resolution Wave mode (ESAHRWVW),<br>Geostationary Operational Environmental (GOESBUFR),<br>Imaging Spectroradiometer (MODIS),<br>Meteosat 2nd Generation satellite winds (MSGWINDS),<br>Satellite Observations (SATOB) | wind<br>wind<br>wind<br>wind<br>wind | 1988-2017 | MO |
| scatwinds | SeaWinds,<br>WindSat,<br>Advanced Scatterometer (ASCAT),<br>High Resolution Advanced Scatterometer (ASCATHR),<br>ESA High Resolution Wave mode (ESAHRWVW),<br>ESA Scatterometer (ESAUWI) | wind | 1992-2017 | ECMWF |
| SEVIRIclear | Meteosat 2nd Generation clear sky radiances (MSGCSR),<br>Meteosat 2nd Generation radiances (MSGRAD) | clear sky | 1982-2017 | ECMWF |
| TOVS | Operational Vertical Sounder | radiances | 1979-2002 | ECMWF |

Table 4: List of observations (Part 2 of2).

| Variable | Model Levels | Pressure Levels | Height Levels |
|---|---|---|---|
| Pressure | X | | X |
| Geopotential height | | X | |
| Temperature | X | X | X |
| U component of wind | X | X | |
| V component of wind | X | X | |
| Wind direction | | | X |
| Wind speed | | | X |
| Cloud Cover | X | X | X |
| Relative humidity | | X | X |
| Specific humidity | X | | |
| Specific cloud ice water content | X | X | X |
| Specific cloud liquid water content | X | X | X |

Table 5: Multi-level field output

### B.5 Precipitation and moisture

Total precipitation, snow fall, total column water vapour.

### B.6 Pressure (single level)

Mean sea pressure and surface pressure.

### B.7 Cloud (single level)

Low cloud cover, medium cloud cover, high cloud cover and total cloud cover.

### B.8 Land

Orography, land-sea mask, surface roughness, snow depth water equivalent, volumetric soil moisture and soil temperature. Volumetric soil moisture and soil temperature are available on four soil levels at depths 0.1, 0.35, 1.0 and 3.0m

## References

[Buizza and Palmer, 1998] Buizza, R. and Palmer, T. N. (1998). Impact of ensemble size on ensemble prediction. *Monthly Weather Review*, 126(9):2503–2518.

[Candy, 2014] Candy, B. (2014). Assimilation of satellite data for the land suface. *ECMWF Annual Seminar Proceedings: Use of Satellite Observations in Numerical Weather Prediction.*

[Davies et al., 2005] Davies, T., Cullen, M. J. P., Malcolm, A. J., Mawson, M. H., Staniforth, A., White, A. A., and Wood, N. (2005). A new dynamical core for the met office's global and regional modelling of the atmosphere. *Q.J.R. Meteorol. Soc*, 131(608):1759–1782.

[Dee, 2004] Dee, D. P. (2004). Variational bias correction of radiance data in the ECMWF system. *Proceedings of ECMWF workshop on assimilation of high spectral resolution sounders in NWP*, pages 97–112.

[Dee et al., 2011] Dee, D. P., Uppala, S. M., Simmons, A. J., Berrisford, P., Poli, P., Kobayashi, S., Andrae, U., Balmaseda, M. A., Balsamo, G., Bauer, P., Bechtold, P., Beljaars, A. C. M., van de Berg, L., Bidlot, J., Bormann, N., Delsol, C., Dragani, R., Fuentes, M., Geer, A. J., Haimberger, L., Healy, S. B., Hersbach, H., Hlm, E. V., Isaksen, L., Kllberg, P., Khler, M., Matricardi, M., McNally, A. P., Monge-Sanz, B. M., Morcrette, J.-J., Park, B.-K., Peubey, C., de Rosnay, P., Tavolato, C., Thpaut, J.-N., and Vitart, F. (2011). The era-interim reanalysis: configuration and performance of the data assimilation system. *Q.J.R. Meteorol. Soc*, 137(656):553–597.

[Dee, 2014] Dee, R. (2014). Use of satellite data in reanalysis. *ECMWF Annual Seminar Proceedings: Use of Satellite Observations in Numerical Weather Prediction.*

[Donlon et al., 2012] Donlon, C. J., Martin, M., Stark, J., Roberts-Jones, J., Fiedler, E., and Wimmer, W. (2012). The operational sea surface temperature and sea ice analysis (ostia) system. *Remote Sensing of Environment*, 116:140 – 158. Advanced Along Track Scanning Radiometer(AATSR) Special Issue.

[Lorenc, 2012] Lorenc, A. (2012). Variational bias correction of observations. *VAR Scientific Paper*, 32.

[Piccolo and Cullen, 2016] Piccolo, C. and Cullen, M. (2016). Ensemble data assimilation using a unified representation of model error. *Mon. Wea. Rev*, 144(1):213–224.

[Rawlins et al., 2007] Rawlins, F., Ballard, S. P., Bovis, K. J., Clayton, A. M., Li, D., Inverarity, G. W., Lorenc, A. C., and Payne, T. J. (2007). The met office global four-dimensional variational data assimilation scheme. *Q.J.R. Meteorol. Soc*, 133(623):347–362.

[Saetra et al., 2004] Saetra, O., Hersbach, H., Bidlot, J.-R., and Richardson, D. S. (2004). Effects of observation errors on the statistics for ensemble spread and reliability. *Monthly Weather Review*, 132(6):1487–1501.

[Titchner and Rayner, 2014] Titchner, H. A. and Rayner, N. A. (2014). The met office hadley centre sea ice and sea surface temperature data set, version 2: 1. sea ice concentrations. *J. Geophys. Res. Atmos.*, 119:2864–2889.

[Unden et al., 2014] Unden, P. et al. (2014). Uncertainties in ensembles of regional reananlyses.

[Wood et al., 2014] Wood, N., Staniforth, A., White, A., Allen, T., Diamantakis, M., Gross, M., Melvin, T., Smith, C., Vosper, S., Zerroukat, M., and Thuburn, J. (2014). An inherently mass-conserving semi-implicit semi-lagrangian discretization of the deep-atmosphere global non-hydrostatic equations. *Q.J.R. Meteorol. Soc*, 140(682):1505–1520.